

# COMMUNICATION CHANNEL INFLUENCE ON SELF INTERFERENCE CANCELLATION FOR IN-BAND FULL-DUPLEX UNDERWATER ACOUSTIC SYSTEMS

Hala A. Naman <sup>1</sup>, A.E. Abdelkareem <sup>2</sup>

<sup>1</sup> College of Engineering, University of Wasit, Iraq

<sup>2</sup> College of Information Engineering, Al-Nahrain University, Baghdad, Iraq

haltaee@uowasit.edu.iq <sup>1</sup>, Ammar.algassab@nahrainuniv.edu.iq <sup>2</sup>

Corresponding Author: A.E. Abdelkareem

Received:16/04/2022; Revised: 14/08/2022; Accepted:16/08/2022

DOI:[10.31987/ijict.6.2.210](https://doi.org/10.31987/ijict.6.2.210)

**Abstract-** Understanding the characteristics of channel propagation is essential for the optimal design of self-interference cancellation (IBFD-UWA) communication systems. UWA channels have propagation characteristics based on the configurations of direct and multipath between a transmitter and a receiver for both self-interference and communication channels. The geometry model and the Bellhop simulator are used to model both channels, respectively, to accommodate any possible changes in the underwater environment. This paper employs self-interference cancellation based on two nodes operating in the IBFD mode, orthogonal frequency division multiplex (OFDM) modulation with quadrature phase-shift keying (QPSK) mapping. By using numerical simulations, it can be shown that the developed model can describe the underwater acoustic environment accurately. The results indicate that local multipath propagation delays can exceed 1.4 s with transmission losses of up to 80 dB. The SIC requires about 4 seconds to reduce SI signals to background noise levels successfully.

**keywords:** Self-interference cancellation, In-Band Full-duplex, SI channel model, Underwater acoustic communication.

## I. INTRODUCTION

Underwater Acoustic (UWA) communication systems deal with many challenges, including delays spread out over a large number of paths. This delay results in inter-symbol interference and spread of the Doppler caused by motion, which dilates the signal severely and leads to bandwidth with intense limitations [1][2]. The main goal of this research is to maximize the capacity of an underwater acoustic system by using a mode of full-duplex communication. Full-duplex means transmitting and receiving over the same frequency band simultaneously, called In-Band Full-Duplex (i.e., IBFD). Furthermore, the IBFD poses some crucial challenges, such as self-interference, where the desired signal is swamped by strong self-interference signals (SI) at the analog-to-digital converter (ADC) due to the strength of the signal. Consequently, suppressing the SI signal prior to the ADC is essential for enabling the FD mode. There is much more to contend with realistic full-duplex UWA systems, which should be considered, and one of them is the variation of channel. Therefore, reliable information regarding the SI channel will be required in order to build these suppression strategies properly [3]. Researchers have worked on self-interference cancellation (SIC) techniques in systems with wireless communication in the past decade [4].

## II. RELATED WORK

There have been limited studies exploring the IBFD in underwater acoustic applications, and some of them are cited here. J. Gibson et al. [5] examined whether FD in UWA communication can be made possible using code-division multiple access

(CDMA). Compared to frequency-division multiple access (FDMA), CDMA techniques are indicated a higher bandwidth efficiency. They use a CDMA scheme and a spread spectrum (SS) technique. G. Qiao et al. [6], showing how to achieve the FD mode in acoustic systems on the basis of orthogonal frequency division multiplexing (OFDM). Moreover, Li et al. [3] presented a procedure for analyzing the path loss of the multipath SI channels used in an acoustic full-duplex system, along with a SIC technique combining digital and analog SIC schemes for the nodes of full-Duplex underwater acoustic systems. A digital method for SI suppression and inter-symbol interference (ISI) elimination combining a soft decision feedback equalizer and a time reversibility scheme was developed by J. Tian et al. [7]. C. Healy et al. [8] investigated the NLMS approach for adaptively estimating a reference signal's amplitude, delay, and phase given previous knowledge of a transmitted signal.

In [9] digital SI cancellation based on RLS adaptive filter repeatedly with dichotomous coordinate descent (DCD) tried in an indoor water tank was described. Furthermore, in [10], it was utilized to identify the influence of the housing at the nearest receiver on the SI using a simplified finite element approach of the IBFD UWA communication modem. Furthermore, the outcomes reveal that the self-loop interference (SLI) signal, which is acquired by the nearest receiver, has diffraction and dispersion components, with the scattering component being much more assertive. An improved so-called maximum likelihood (ML) approach for estimating SI channels is used, with a sparsity penalty including the cost function, to get acceptable SI channel estimations. This was proposed by G. Qiao et al. [11]. Seawater transmission and reflection losses at the seabed were taken into consideration by C. Healy et al. [12] to define the SI channel CIR taps. Reverberations in shallow water may endure more than a second due to surface and subsurface reflections.

### III. CONTRIBUTION

Research into the challenges associated with the mode of an FD in UWA communication is critical to a better understanding of the operational issues. The variable and moving channels underwater are among the main obstacles which cause not only FD modem reflections from the seafloor and surface but also multipath reflections from these surfaces for both SI channel and communication channel. Therefore, the calculation of the time delay and transmission loss of the two SI and communication channels is essential in determining the received signal from the distant node, which is reconstructed based on the detected signal, which the SIC subtracts from the incoming signal after the SIC to produce the remaining SI signal, which must be fed into the NLMS algorithm. The following is the structure of this paper: The system model is discussed in Section 4. Section 5 includes simulation results. Lastly, conclusions are made in Section 6 of the article.

### IV. SYSTEM MODEL

This section presents the In-Band Full-Duplex UWA system architecture that consists of a receiver that receives near-transmitted signal passed through the SI channel and a transmitter that transmits far-transmitted signal passed through the communication channel and noise.

#### A. *Transmitter System*

Two different nodes of underwater acoustics employing OFDM and a modulation method of quadrature phase-shift keying (QPSK) are considered for transferring the information over IBFD. The inversed discrete Fourier transform (IDFT)

with  $k$  points has been used for calculating the signal in order to transfer time-domain information gleaned from the closest node on the symbols of the  $k$ 'th QPSK block, denoted by  $X_1(k)$  as follows:

$$x_1(n) = \frac{1}{\sqrt{K}} \sum_{k=0}^{K-1} X_1(k) e^{j\frac{2\pi nk}{K}}, n = 0, 1, \dots, N - 1 \quad (1)$$

Where  $x_1$  is implemented with the guard intervals in the beginning to accommodate multipath induced ISI. The guard intervals are added to the beginning of the original sequences after adding the last  $L_{CP}$  samples of  $x_1$ , which are also known as the cyclic prefix (CP). A multipath channel will exhibit an excessively delayed spread,  $L_f$ , if the impulse response between two nodes is  $h_f$ . According to the proposed system, it is assumed that  $L_{CP} \geq L_f$ . Therefore, the transferred block of orthogonal frequency division multiplexing can be expressed by:

$$x_{1CP} = [x_1(K - L_{CP}), \dots, x_1(K - 1), x_1(0), \dots, x_1(K - 1)]^T \quad (2)$$

The data is transmitted over the SI channel between the nodes. Channel modeling and empirical measurements will be discussed in the following section. The parameters of the transmitted OFDM signal are indicated in Table I, and the baseband and passband of the transmitted signal are shown in Fig. 1 (a) and (b), respectively.

TABLE I  
 OFDM Signal Parameters

Bandwidth B	6kHz
Number of sub-carrier $N_c$	2048
Number of bits per subcarrier	2 (QPSK bit)
Maximum Delay Spread	12 ms
Symbol duration	256 ms
CP interval	72
Carrier frequency	12kHz
Sampling frequency	48kHz

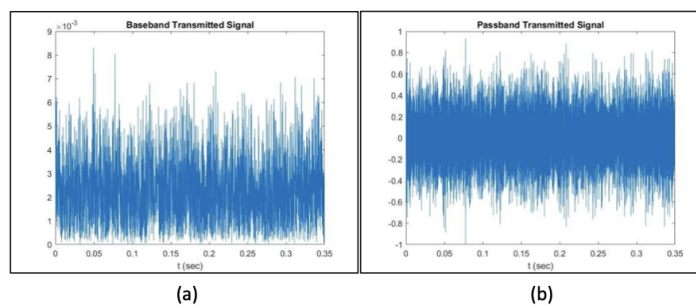


Figure 1: Transmitted OFDM Signal (a) Baseband, (b) Passband

### B. Modeling of Underwater Acoustic Channels

Oceanic channels are considered one of the most challenging transmission mediums, and acoustic signals are ideal for underwater communication and transmitter construction. Acoustic signals are prone to various losses, including absorption, scattering, multipath propagation, and Doppler shifts. The transmission pattern and distance traveled by an acoustic signal in seawater are estimated using experimental modeling of underwater channels. The far-end node interface sends the intended signal to the FD-UWA system's hydrophone, along with signals from the near-end receiver, along with various surfaces and bottom reflections, as well as noise. An acoustic communication scenario in shallow water is depicted in Fig. 2, where the first is a self-interference channel between the transmitter and receiver in the same node, and the second is a communication channel between near and far nodes, which are explained in this section.

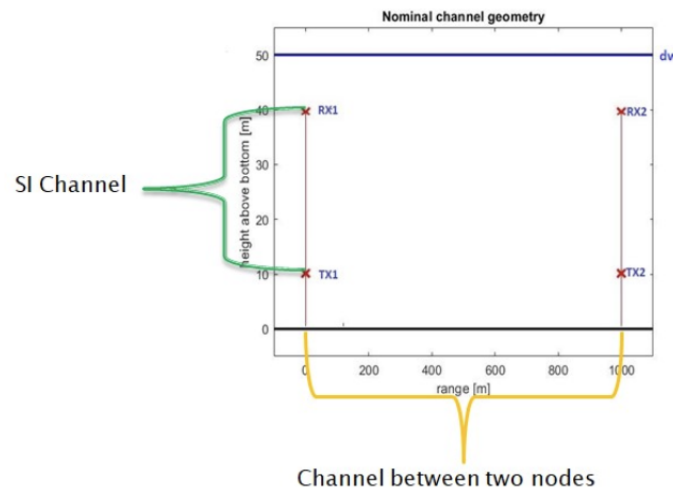


Figure 2: An Acoustic Communications Scenario in Shallow Water

#### 1) Same node SI channel Modeling

As mentioned previously, several surfaces, bottom reflections, and noise in the FDUWA system's hydrophone were received with the intended signal, together with signals from the near-end receiver. Since the direct path's high power and multipath latency might exceed one second, they must not be ignored [13]. To implement a basic model of the vertical channel, one must consider the self-interference propagation delay of the channel, spreading, transmission, and loss due to absorption. Inter-symbol interference (ISI), a little Doppler interference, and some other types of interference have been produced as a result of the time-varying nature of multipath channels. The transmission loss ( $TL$ ), measured in decibels (dB), is the metric that quantifies the reduction in intensity as a function of distance traveled. The spread loss and attenuation are combined to produce the transmission loss quantified using Eq. (3) [13]. The latter would be generated by the unavoidable frictional conversion of sound into heat that occurs throughout the transmission of sound waves as described below:

$$TL(f) = 2\alpha_z + k \log_{10}(r) + a(f)r \quad (3)$$

In this case,  $\alpha_z$  represents the attenuation in the  $zy$  and  $zx$  planes and is  $\alpha_z \approx -15$  dB as a result of the employment of toroidal transducers with a beam pattern in both the transmitter and the receiver. The parameter  $r$  denotes the propagation distance ( $m$ ), and  $k$  indicates the spreading factor, which takes 10 for spherical spreading and 20 for free-field spreading. In this work, a realistic expression between the spherical and cylindrical laws is chosen as the basis; the following relations hold:

$$\alpha(f) = \alpha_1 + \alpha_2 + \alpha_3 \quad (4)$$

$$\alpha_1 = af^2 \text{ (Freshwater attenuation)} \quad (5)$$

$$\alpha_2 = bf_0 / \left(1 + (f_0/f)^2\right) \text{ (MgSO}_4 \text{ Relaxation )} \quad (6)$$

$$\alpha_3 = cf_1 / \left(1 + (f_1/f)^2\right) \text{ (Boric acid relaxation)} \quad (7)$$

$$a = 1.3 \times (10 * (-7)) + 2.1 \times ((10 * e(-10))(T - 38))^2 \quad (8)$$

$$b = 2S \times (10 * (-5)) \quad (9)$$

$$f_0 = 50 \times (T + 1) \quad (10)$$

$$c = 1.2 \times 10^{-4} \quad (11)$$

$$f_1 = (10)^{(T-4)/100} \quad (12)$$

In this equation,  $S$  specifies salinity ( $hr$ ),  $T$  means, the temperature, in  $^{\circ}C$ , and  $f$  is operating frequency  $kHz$ .

A vertical SI channel's propagation environment in IBFD shallow water is characterized as a triangle for multipath reflection dispersed throughout the sea's top and bottom [14]. The path of propagation from a transmitter to a receiver is calculated using the right triangle theorem for both direct and multipath propagation. The hypotenuse of each reflection mirrors the corresponding propagation time. Surface reverberation is assumed to be one type of reverberation, with the first

reflection coming from the surface of the object. The second reflection comes from the bottom, mirroring the first. The propagation path of the straight path delay  $T_D$  is described via the following relations [14] :

$$T_D = (D_T - D_R) / c \quad (13)$$

While the propagation delay for each reflection from surface and bottom is described as:

$$T_{Sn} = \left( \sqrt{(D_T - D_R)^2 \tan^2 \theta + \left( D_T + \left\lfloor \frac{n}{2} \right\rfloor 2D_W + (-1)^{n+1} D_R \right)^2} \right) / c \quad (14)$$

$$T_{Bn} = \left( \sqrt{(D_T - D_R)^2 \tan^2 \theta + \left( \left\lfloor \frac{n}{2} \right\rfloor 2D_W - (D_T + (-1)^{n+1} D_R) \right)^2} \right) / c \quad (15)$$

Where n from 1 to N and transmitter depth calculated by:

$$D_T = L * \cos(\theta) \quad (16)$$

In this case, the transmitter and receiver depths are denoted by  $D_T$  and  $D_R$ , respectively. Depending on  $L$ , the transmitter and receiver distance ( $D_T$ ) will change. The FD and water column's angles are denoted by  $\theta$ . Moreover, indicates water depth, and  $c$  refers to sound speed. Fig. 3 displays the predicted propagation delay for a single reflection.

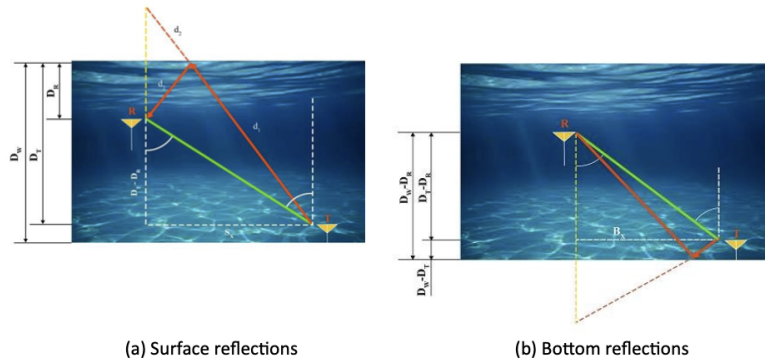


Figure 3: Multipath Reflections in SI Channel

The hydrophone and transducer configuration with one side of a UWA-IBFD communication simulation is depicted in Fig. 4. At a depth of approximately 40( m), the transmitter is situated. The transducer is 30( m) away from the hydrophone, and the depth of the lake in the testing region is around 50( m).

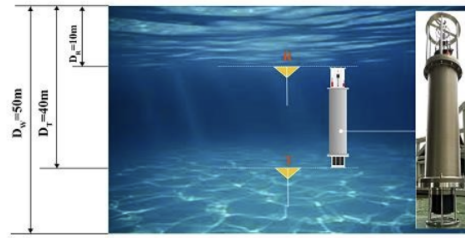


Figure 4: Simulation Setup of the System

While the coefficient of pressure reflection at the sea surface margins is nearly  $a \approx -1$  and, the coefficient of pressure reflection at the seabed is about  $b \approx 1$  [14]. At the receiving end, the uniform surface reflections increase, whereas the uneven surface and bottom reflections decrease.

With transmission parameters,  $f = 12\text{kHz}$ ,  $k = 15\text{kHz}$ , and temperature  $T = 14^\circ\text{C}$ , the resulting delay and transmission loss for  $N = 40$  are shown in Fig. 5 for angle  $\theta = 0$ .

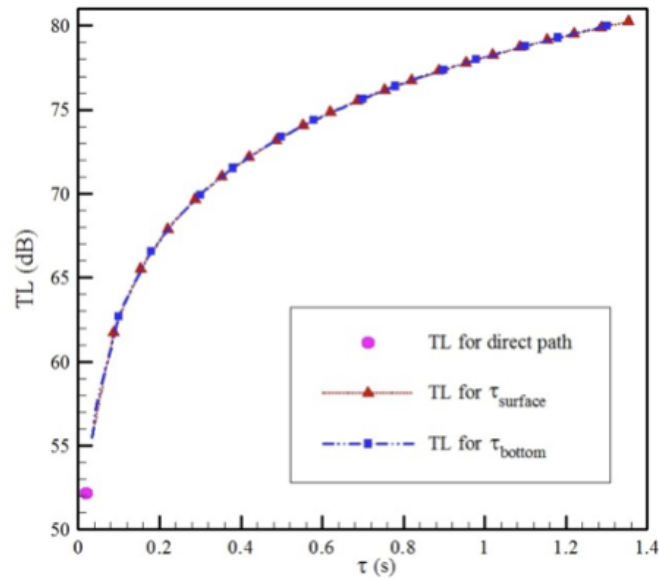


Figure 5: The Multipath Propagation Transmission Loss When  $\theta = 0^\circ$ .

The related impulse responses are seen in Fig. 6 for deviating from the vertical direction in the SI channel. It is worth noting that in practice, it is expected that beyond the normally incident waves, signal waves with small angles (with respect to  $z$  axis) will be additionally propagated, which results in a more diffuse impulse response.

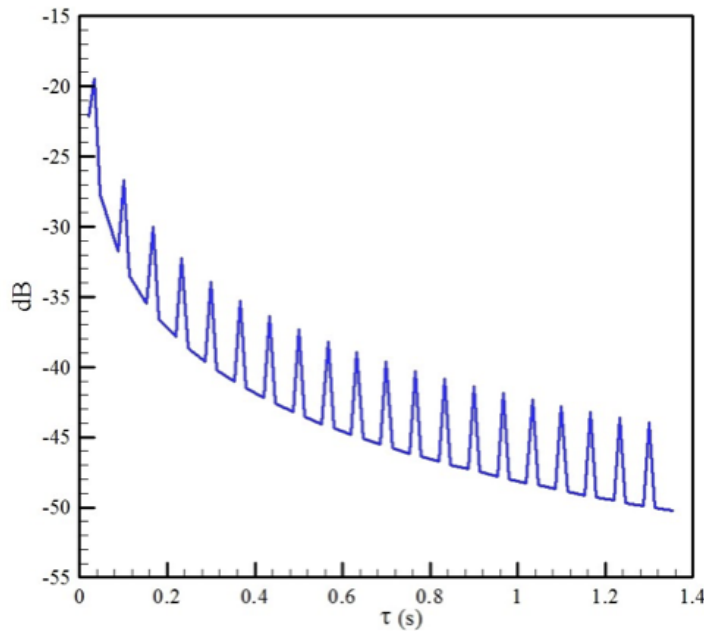


Figure 6: Self-interference Channel Response When  $\theta = 0^\circ$ .

## 2) Two nodes channel Modeling:

BELLHOP [15], which is designed by M. Porter and maintained by [16], is used to model channel behavior and is freely accessible as a component of the Acoustics Toolbox. In ray theory, acoustic waves are modeled as a series of rays that flow in specific directions from the sender to the receiver [17]. A beam adds a Gaussian intensity profile to the ray trajectory, allowing for more accurate computations of total acoustic intensity at any given place in space [18]. Acoustic wave propagation may be accurately obtained using the beam tracing method when the curvature of the ray trajectory and the variation in acoustic pressure amplitude over a single wavelength is insignificant [19]. BELLHOP beam tracing outputs may be used to synthesize accurate impulse responses of multipath channels in UWA, and these simulated channels can be used to determine properties of received signals, such as the amplitude and latency of received signals. Because of these adverse characteristics of the underwater acoustic (UWA) communication medium, UANs' performance is severely limited compared to terrestrial radio systems [20]. The sound speed is typically between 1450 and 1550 m/s, and the bandwidth is in the several kHz range, with a large multipath delay spread and Doppler effect.

a) Characteristics of the UWA channels In this section, the significant properties of the UWA channel are presented as they apply to underwater acoustic channel design.

### – Sound speed:

The slow speed of sound propagation is the most important physical issue influencing the performance of underwater channel measurements. Acoustic waves travel at a pace of roughly 1500 m/s over water, which is a factor of  $2 \times 10^5$  slower than terrestrial radio networks, which travel at  $3 \times 10^8$  m/s. Furthermore, water temperature, pressure, and salinity

alter the sound speed and make it changeable within time and space [21], as depicted in Fig. 7. As can be observed, it describes a depth-dependent sound speed profile (SSP).

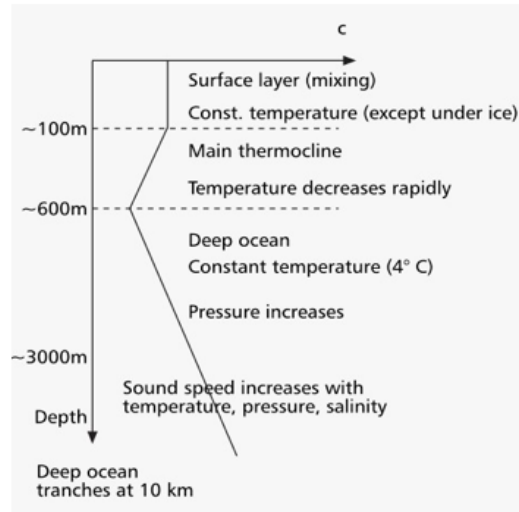


Figure 7: Sound Speed Profile [22]

Accordingly, the sound speed profile leads to curved wave propagating paths due to the refraction of acoustic waves. BELLHOP simulated underwater acoustic signal propagation with refraction.

– Multipath propagation:

Multipath structures in the UWA Channel are influenced by the sea surface [23]. Sound waves are reflected off the sea surface, and the seafloor is shifted 180 degrees. The result may be interference from multipath reflection from the seafloor and surface. The Bellhop simulator is able to integrate the sea surface and the natural seafloor into raytracing modeling by considering the roughness of the sea surface and bathymetry, or the features of the seabed, to generate more realistic scattering patterns. It would work properly if the UWA waves were scattered so that some paths moved towards the seafloor and gradually refracted upwards.

Conversely, upward sound propagates until it encounters a robust positive sound speed gradient, which makes it refract downward. Signals may also be reflected off the water surface and received by the receiver. This modeling predicts that the broadcast signal will arrive at different locations with random surface waves. Bellhop also describes quite complex interactions occurring between acoustic waves and sediments on ocean bottoms. Depending on the incident angle, acoustic waves attenuate and modify the phase of the sound that passes through the soil layer. The degree of acoustic wave absorption and reflection by sediment layers depends on particle size, porosity, grain density, and gas concentration [24]. In the case of rays, an energy profile is more broadly distributed by using the Gaussian intensity profile. A more accurate way to simulate the UWA multipath propagation Gaussian beam spread is to superimpose multiple Gaussian beams within the

receiver's region. This approach provides a more accurate representation of the overall acoustic intensity at the receiver [25], as demonstrated in Fig. 8 (a) and (b) for the proposed scenario.

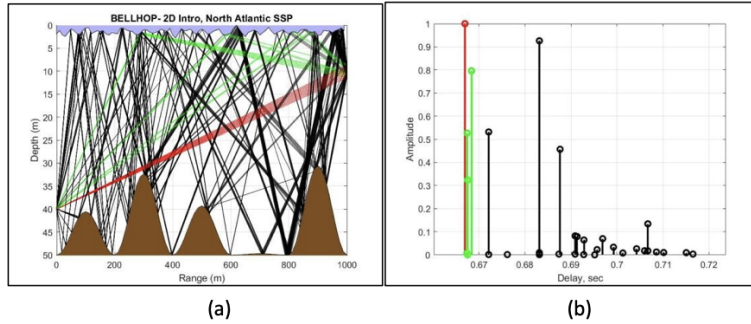


Figure 8: The Amount Of Ray-Traced Multipath Components at the Receiver Increases Significantly Due to the Sea Surface and Bottom Roughness.

– Spreading and absorption loss:

Absorption and geometric spreading induce the underwater attenuation of acoustic signal power, which may be calculated as follows [26]:

$$L(d, f) = L_{spr}(d) + d_{km}L_{abs}(f) \quad (17)$$

Where  $L(d, f) = 10 \log(P_{rx}/P_{src})$  is the power loss in decibels, which can be described as the ratio of received power  $P_{rx}$  to source power  $P_{src}$  and varies with distance  $d$  and frequency  $f$ . Moreover,  $abs(f)$  denotes the losses per kilometer attained by absorption [ dB/km ] at the frequency of  $f$ kHz. Besides,  $d_{km} = d \times 10^{-3} = d$  is the distance (km), and  $L_{spr}(d)$  is the spreading loss parameter at  $d$  meters from the source. The spread loss parameter is calculated via the following relation:

$$L_{spr}(d) = k \times 10 \log\left(\frac{d}{d_{ref}}\right) \quad (18)$$

where the exponent  $k[1, 2]$  specifies the geometry of the propagation.  $k = 1$  is the default setting in which water depth is much shorter than the horizontal transmission range, and spreading is cylinder-shaped, as opposed to the spherical spreading described by  $k = 2$  signifies terrestrial radios loss in free space path systems. Equation (18) divides the distance by a reference distance  $d_{ref}$  to indicate the spreading loss in relation to the signal strength at a distance  $d_{ref}$  from the source. Thorp's empirical method developed from ocean measurement data is frequently used to calculate absorption loss if the frequency exceeds a few hundred Hz [26]:

$$L_{abs}(f) = 0.11 \frac{f^2}{1 + f^2} + \frac{44f^2}{4100 + f^2} + 3 \times 10^{-4} f^2 + 3.3 \times 10^{-3} \quad (19)$$

The transmission loss for the proposed model at 12 kHz frequency is shown in Fig. 9.

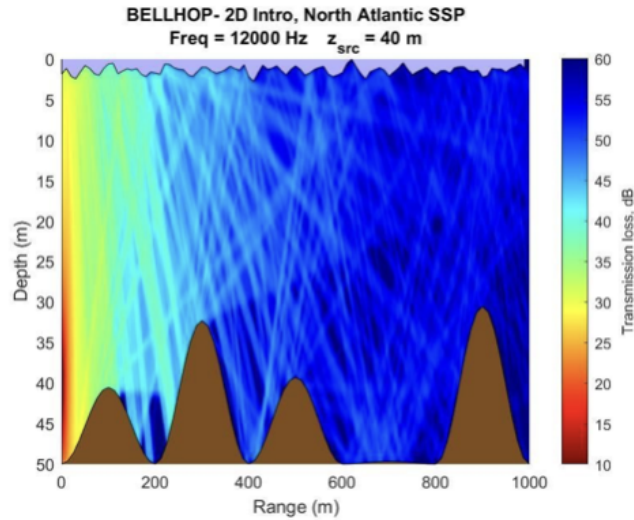


Figure 9: Transmission Loss Results From the Dispersion and Absorption of a Signal

### C. The structure of the receiver

At the local node, the received signal can be described as:

$$y(n) = s_f(n) + s_{SI}(n) + w(n) \quad (20)$$

where  $s_f$  and  $s_{SI}(n)$  indicate the received signal from the far node and the Selfinterference signal, respectively. They can be written as follows:

$$s_f(n) = \sum_{m=0}^{M-1} h_f(n-m)x_f(m) \quad (21)$$

$$s_{SI}(n) = \sum_{p=0}^{P-1} h_{SI}(n-p)x_{SI}(p) \quad (22)$$

The ambient noise is indicated by  $w(n)$ .

Consequently, the SI signal has to be successfully suppressed before the ADC, allowing the receiver to identify the signal of interest  $s_f(n)$ . Otherwise, the SI signal at the ADC would drown it. The detection of the SI signal is effectively suppressed in [8] by the SIC approach in combination with the node design. It is illustrated in Fig. 10 that with the help of an adaptive filter,  $h_{SI}$ , the IBFD-underwater acoustic communication node constructs a replication of the SI signal,  $cs(n)$ , using its complete knowledge of the transmitted signal such that:

$$cs(n) = \hat{h}_{SI}^H x(n) \quad (23)$$

The Hermitian transposition is denoted by  $(\cdot)^H$ . The adaptive filters have a length equal to the SI channel length,  $L_{SI}$ . The output of the adaptive filter,  $cs(n)$ , is subtracted from the received signal is carried out in order to reduce the SI signal's impact on the ADC expressed as:

$$y_l(n) = s(n) + r_l(n) + w(n) \quad (24)$$

where  $r_l(n)$  denotes the residual SI after the SIC:

$$r_l(n) = s(n) - cs(n) \quad (25)$$

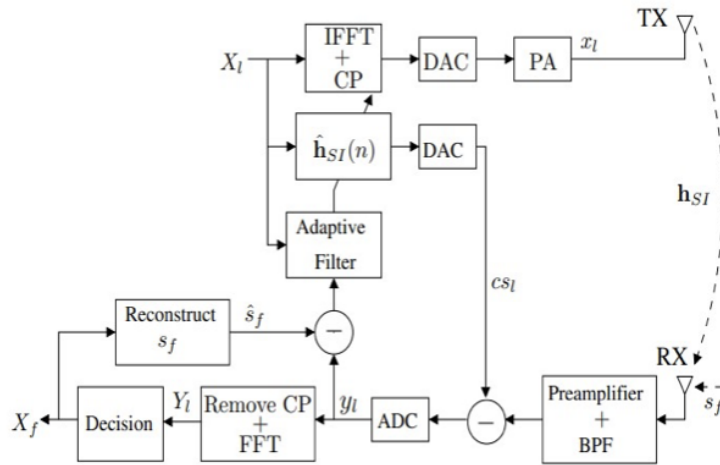


Figure 10: The Planned IBFD-UWA Nodes Architectural Design[8].

The frequency-domain signal which is received within the frequency domains is formed by eliminating the CP and implementing a discrete Fourier transform (DFT).

$$Y_l(k) = S(k) + R_l(k) + W(k) \quad (26)$$

Where  $(k)$ ,  $R_l(k)$ , and  $W(k)$  signify the frequency domain's representation of the signal of interest, residual SI, and ambient noise, respectively, and  $k$  indicates the subcarrier index. A zero-force equalizer and maximum likelihood detection are used to identify the signal coming from the distant node,  $X_f(k)$ . The channel among the nodes is analyzed using frequency response information.

$$Y_{zf}(k) = \frac{S_f(k)}{H(k)} + \frac{R_l(k)}{H(k)} + \frac{w(k)}{H(k)} \quad (27)$$

where  $(k) = H(k)X_r(k)$ . Using ML detection, one can obtain  $X_f(k)$  as:

$$\hat{X}(k) = \underset{(q) \in \mathbb{Z}M}{\operatorname{argmin}} |Y_{zf}(k) - H(k)\mathcal{C}(q)|^2 \quad (28)$$

The constellation vector QPSK is indicated by  $\mathcal{C}$ . As part of an adaptive SIC technique, Eq. (25), the residual SI after SIC will be collected and sent to the NLMS algorithm to monitor variations in the SI channel. Based on the ML detection output, one can reconstruct the received signal received;  $S_f$  based on the channel's frequency response between the nodes:

$$\hat{s}_f(n) = \frac{1}{\sqrt{K}} \sum_{k=0}^{K-1} H(k)\hat{X}_r(K)e^{j\frac{2\pi nk}{K}} \quad (29)$$

After subtracting the received SI signal from the residual SI signal, one may calculate the SI signal residual Eq. (26).

$$RS(n) = s_f(n) - \hat{s}_f(n) + r(n) + w(n) \quad (30)$$

A signals estimated version is given by (n) and takes the form:

$$\hat{s}_f(n) = s_f(n) + \epsilon_{sr}(n) \quad (31)$$

The adaptive SIC approach uses the residual SI signal to track variations in the SI channel Eq. (30). Based on [27], the adaptive SIC's NLMS method updates the tap-weight vector,  $h(n+1)$ , based on the residual SI signal Eq. (30). The resulting trace is used to generate the replica as  $cs(n)$  which is expressed via the following relation:

$$\hat{h}_{SI}(n+1) = \hat{h}_{SI}(n) + \frac{\tilde{\mu}}{\delta + \|x_l(n)\|^2} x_l(n)RS^*(n) \quad (32)$$

Where  $0 < \delta \leq 1$  and  $\mu$  denotes an adaptation constant.

## V. RESULTS

The result of using IBFD-UWA communication system-based OFDM with a QPSK modulation method is presented here. Employing the channel model of the same node and between two nodes as described in Section B. The received signal consists of transmitted signals from near and far nodes in addition to the noise. It should be noted, as shown in Fig.11, that the remote node signal is considerably weaker than the SI signal. As a result, the SI signal must be suppressed effectively before the ADC in order for the receiver to recognize the signal of interest. Otherwise, the ADC's SI signal would drown it out. Fig. 12 shows the power of the residual SI after the SIC. As can be seen in more detail in this figure, the suggested SIC successfully reduces SI signals to background noise levels (90 dB) to enable the signal of interest to be detected correctly by the receiver.

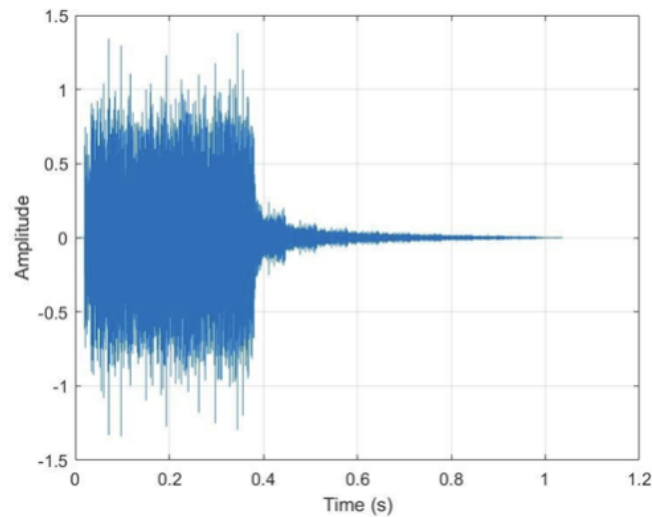


Figure 11: The Received Signal From the Local Node and Distant Node

Also, by comparing new results with the existing works, the system requires roughly 4 seconds to suppress the self-interference to noise level, while researchers in [8] need 6 sec for that.

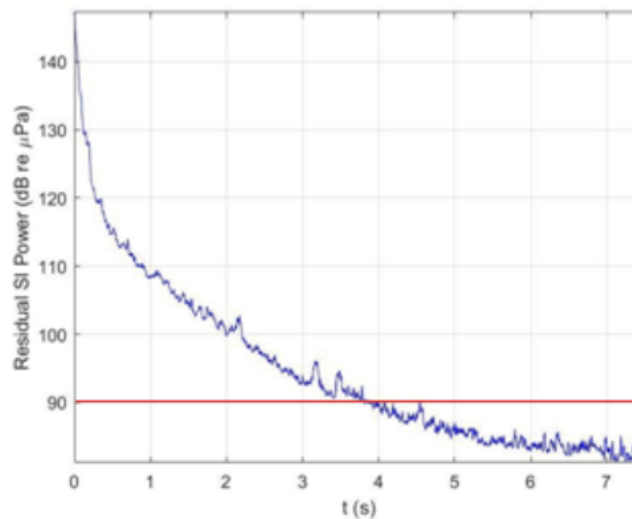


Figure 12: The Power Of the Residual SI Signal After the SIC Has Been Adaptively Applied

## VI. CONCLUSION

In this paper, in order to define IBFD-UWA nodes that successfully reduce SI signals before they reach the local ADC, the angle of the FD modem's orientation and the vertical column of water are used. A model for SI channels and

communication channels is adopted in this study. The loss of seawater transmission and the arrival time of reflections between the seabed and surface are taken into account when estimating the channel's output CIR taps. In shallow water, the developed model properly interprets the performance of the SI channel, as demonstrated by the simulations. The SIC technique performs well when the signal of interest is taken into consideration along with its inherent channel delay and loss.

## Funding

None

## ACKNOWLEDGEMENT

The author would like to thank the reviewers for their valuable contribution in the publication of this paper.

## CONFLICTS OF INTEREST

The author declares no conflict of interest.

## REFERENCES

- [1] Z. Guo, A. Song, M. Towliat, L. J. Cimini, X.-G. Xia, and C.-C. Shen, "Self interference Characterization for In-Band Full Duplex Underwater Acoustic Communications," in Proceedings of the International Conference on Underwater Networks & Systems, 2019, pp. 1-5.
- [2] A. E. Abdelkareem, B. S. Sharif, and C. C. Tsimenidis, "Adaptive time varying doppler shift compensation algorithm for OFDM-based underwater acoustic communication systems," *Ad Hoc Networks*, vol. 45, pp. 104-119, 2016, DOI: 10.1016/j.adhoc.2015.05.011.
- [3] L. Li, A. Song, L. J. Cimini, X.-G. Xia, and C.-C. Shen, "Interference cancellation in inband full-duplex underwater acoustic systems," in OCEANS 2015-MTS/IEEE Washington, 2015, pp. 1-6.
- [4] S. Cancellation, *Full-Duplex Wireless Communications Systems*. 2017.
- [5] G. G. X. J. H. Gibson and K. Bektas, "Evaluating the Feasibility of Establishing Full Duplex Underwater Acoustic Channels," *Channels*, vol. 5, p. 7, 2004.
- [6] G. Qiao, S. Liu, Z. Sun, and F. Zhou, "Full-duplex, multi-user and parameter reconfigurable underwater acoustic communication modem," in 2013 OCEANSSan Diego, 2013, pp. 1-8.
- [7] J. Tian, S. Yan, L. Xu, and J. Xi, "A time-reversal based digital cancellation scheme for in-band full-duplex underwater acoustic systems," *Ocean. 2016 - Shanghai*, pp. 03, 2016, doi: 10.1109/OCEANSAP.2016.7485471.
- [8] C. T. Healy, B. A. Jebur, C. C. Tsimenidis, J. Neasham, and J. Chambers, "In-Band Full-Duplex Interference for Underwater Acoustic Communication Systems Bilal," *Ocean. 2019 - Marseille*, pp. 1-5, 2019, DOI: 10.1109/oceanse.2019.8867454.
- [9] L. Shen, B. Henson, Y. Zakharov, and P. Mitchell, "Digital self-interference cancellation for full-duplex underwater acoustic systems," *IEEE Trans. Circuits Syst.. II Express Briefs*, vol. 67, no. 1, pp. 192-196, 2019.
- [10] Y. Zhao, G. Qiao, S. Liu, Y. Zakharov, and N. Ahmed, "Self-interference channel modeling for in-band full-duplex underwater acoustic modem," *Appl. Acoust.*, vol. 175, p. 107687, 2021, DOI: 10.1016/j.apacoust. 2020.107687.
- [11] G. Qiao, S. Gan, S. Liu, and Q. Song, "Self-Interference Channel Estimation Algorithm Based on Maximum-Likelihood Estimator in In-Band Full-Duplex Underwater Acoustic Communication System," *IEEE Access*, vol. 6, no. c, pp. 62324-62334, 2018, DOI: 10.1109/ACCESS.2018.2875916.
- [12] C. T. Healy, B. A. Jebur, C. C. Tsimenidis, J. Neasham, and J. Chambers, "Experimental Measurements and Analysis of In-Band Full-Duplex Interference for Underwater Acoustic Communication Systems," in OCEANS 2019 - Marseille, 2019, pp. 1-5, DOI: 10.1109/oceanse.2019.8867454.
- [13] R. F. W. Coates, *Underwater Acoustic Systems*, vol. 29, no. 4. 1991.
- [14] H. A. Naman and A. E. Abdelkareem, "Variable direction-based self-interference full-duplex channel model for underwater acoustic communication systems," *Int. J. Commun. Syst.*, p. e5096, 2022.
- [15] M. Porter, "The bellhop manual and user's guide: Preliminary draft," *Heat, Light. Sound Res. Inc., La Jolla, ...*, pp. 1-57, 2011, [Online]. Available: <http://oalib.hlsresearch.com/Rays/HLS-2010-1.pdf>.
- [16] N. Morozset al., "Channel Modeling for Underwater Acoustic Network Simulation," pp. 1-25, 2020, DOI: 10.24433/CO.1789096.v1.
- [17] J. C. Peterson and M. B. Porter, "Ray/beam tracing for modeling the effects of ocean and platform dynamics," *IEEE J. Ocean. Eng.*, vol. 38, no. 4, pp. 655-665, 2013, DOI: 10.1109/JOE.2013.2278914.
- [18] J. C. Peterson and M. B. Porter, "Ray/beam tracing for modeling the effects of ocean and platform dynamics," *IEEE J. Ocean. Eng.*, vol. 38, no. 4, pp. 655-665, 2013, DOI: 10.1109/JOE.2013.2278914.
- [19] W. S. Burdick, "Underwater acoustic system analysis, 1991," Prentice Hall. Thorp, WH, *Deep Ocean sound attenuation sub low kilocycle per Second Reg. J. Acoust. Sot. Am*, vol. 38, p. 648, 1965.
- [20] J. Heidemann, M. Stojanovic, and M. Zorzi, "Underwater sensor networks: Applications, advances and challenges," *Philos. Trans. R. Soc. A Math. Phys. Eng. Sci.*, vol. 370, no. 1958, pp. 158-175, 2012, doi: 10.1098/rsta. 2011.0214.
- [21] E. R. Anderson, "Sound Speed in Seawater as a Function of Realistic Temperature Salinity-Pressure Domains," no. August, pp. 1-58, 1971.
- [22] M. Stojanovic and J. Preisig, "Underwater Acoustic Communication Channels: Propagation Models and Statistical Characterization," *IEEE Commun. Mag.*, vol. 47, no. 1, pp. 84-89, 2009, DOI: 10.1109/MCOM.2009.4752682.

- [23] N. Morozs, P. Mitchell, and Y. V. Zakharov, "TDA-MAC: TDMA Without Clock Synchronization in Underwater Acoustic Networks," IEEE Access, vol. 6, pp. 10911108, 2017, DOI: 10.1109/ACCESS.2017.2777899.
- [24] R. D. Stoll and A. C. Kibblewhite, " Sediment Acoustics," J. Acoust. Soc. Am., vol. 88, no. 5, pp. 2507-2508, 1990, DOI: 10.1121/1.400058.
- [25] P. A. Baxley, H. Bucker, V. K. McDonald, J. A. Rice, and M. B. Porter, "ShallowWater Acoustic Communications Channel Modeling Using Three-Dimensional Gaussian Beams," Commun. Syst. Technol., pp. 251-261, 2001.
- [26] M. Stojanovic, "On the relationship between capacity and distance in an underwater acoustic communication channel," WUWNet 2006 - Proc. First ACM Int. Work. Underw. Networks, vol. 2006, pp. 41-47, 2006, DOI: 10.1145/1161039.1161049.
- [27] S. Haykin, Adaptive filter theory, vol. 29, no. 2. 2008.